FICTITIOUS-DOMAIN SIMULATIONS OF BEDLOAD TRANSPORT; FREE-SURFACE FLOW IN A ROTATING TUMBLER

Hung TRUONG[1], Anh NGUYEN[2], Hiroyuki SUGIMOTO[3] and John WELLS[4]

[1]Member of JSCE, Graduate student, Dept. of Civil and Environmental Engineering, Ritsumeikan University, (Noji Higashi 1-1-1, Kusatsu, Shiga 525-8577, Japan)

[2]Graduate student, Dept. of Civil and Environmental Engineering, Ritsumeikan University

[3] Machining Instructor, Dept. of Civil and Environmental Engineering, Ritsumeikan University

[4]Member of JSCE, Associate Professor, Dept. of Civil and Environmental Engineering, Ritsumeikan University

We numerically simulate "bedload transport" of noncohesive sediment by a turbulent liquid flow over an erodible bed using a "fictitious domain" simulation method that employs a fixed Cartesian grid. We report here on comparison with a challenging dense-phase particulate flow, namely a rotating drum partially-filled with spherical particles, through which oil flows to form a free-surface flow . Overall agreement between experimental and simulated values for bed and free-surface angles is found to be quite satisfactory..

Key Words **:** *bedload transpor, ,free surface flow, numerical simulation, turbulence, DEM, rotating drum*

1. INTRODUCTION

To resolve the complex motion of particles in "bedload transport" of sediment requires tracking *O*(1000) 3D particles in the manner of Particle Dynamics Simulations[1),2),3),4)]. Given the absence of reliable turbulence models for dense two-phase flow, one should resolve all stress-supporting scales of the turbulence. Additionally the instantaneous local flow around particles should be resolved, so that point models of fluid force, the accuracy of which is very doubtful in the context of bedload transport, are not required. To simulate such detail, we are developing the efficient "fictitious domain" technique for application to bedload transport, as described in section 2. In an earlier experimental check of our simulation method[5)], we considered a rotating drum half-filled with spherical particles. The present report extends that work by circulating oil to maintain a free-surface flow inside the rotating tumbler. As compared with the simple rotating drum, the particle flow is now driven by a turbulent shear flow, rather than by the immersed weight of the particles, and can thus be considered a form of "bedload transport". As far as we know, this is the first report of such an "open" rotating tumbler, and certainly represents its first application as a benchmark for particle dynamics simulations. Because the flow is far from equilibrium, we believe that this test provides a good complement to standard data bases obtained in straight open-channels.

2. NUMERICAL SIMULATION

We are interested in the scientifically important transition from hydraulically smooth to rough sediment beds, which corresponds to particle Reynolds numbers, based on relative velocity, from 10 to a few hundred. In the upper half of this range, the requirements set out in the last section impose a lower limit on resolution of *O*(10) grid points per diameter. Realistic computing resources do not yet suffice to apply boundary-fitted techniques to thousands of moving particles in 3D, so we must exploit fixed-grid "fictitious-domain" techniques; a standard incompressible Navier-Stokes solver is applied on a uniform Cartesian grid, but is modified to recover rigid body motion inside the moving and rotating particles by adding body forces to the governing equation.

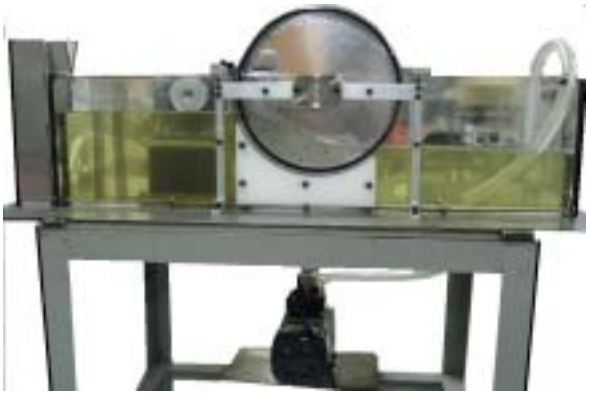

Fig. 1 Photograph of the the rotating drum and flow tanks. Drum turns clockwise, flow of oil is from left to right. Backflow is prevented by the white block under the drum, and by black O-rings between the drum and flow tank.

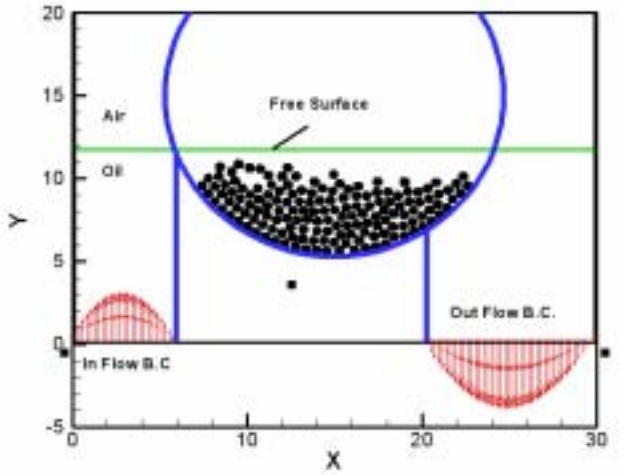

Fig. 2 Setup of computational domain and boundary conditions.

Within the fictitious domain framework, Kajishima[6] has proposed to simply force the velocity field, to match rigid motion within particles, in proportion to the solid volume fraction in a given momentum cell. This efficient algorithm has permitted calculating the motion of 1000 or more solid particles in a turbulent flow, with particle Reynolds number in the range 10~300. Even at the rough resolution of 8 to 10 grid points per particle, Kajishima reports values of drag past a fixed sphere that approximate experimentally observed values well over a wide range of *Re*. Subsequent work[7),8)] has shown that forcing at Lagrangian markers at the particle surface and within the particle achieves greater accuracy, but at a significant cost in computational time. Accordingly, Truong et al. [9)] have combined marker and volumetric forcing; the former is applied at particle surfaces, the latter within particles. In this way, the no-slip condition at particle surfaces is better satisfied than with pure volumetric forcing, but at modest computational cost. Since the effects of particle acceleration should be important during interparticle collisions and vortex entrainment, we apply a variable-density incompressible flow solver; tests reported in that work[9)] showed that this approach does indeed predict particle acceleration better than when using a constant-density solver as done by previous workers.

(1) Computational setup

The freely flowing surface rotating drum apparatus, which contains solid particles, air and oil (see Fig. 1) is modeled as a cylindrical region embedded in a Cartesian computational grid (cf. Fig. 2). The drum boundary and the interface between gas and liquid are represented as two sets of discretized markers that are distributed over the drum surface and the interface, respectively. The distance between two connected markers is set to half or one grid spacing. The gas-liquid interface is assumed to be flatted at the initial stage. The region above the interface is filled with a fluid of low density relative to that of air while the region below the interface is filled with sunflower oil. The pump is modeled by inflow and outflow boundary conditions at the bottom of the computational domain for up and down stream, respectively.

(2) Particle- Fluid interaction

The interaction between particle and fluid phase is solved by a volumetric velocity-based forcing, called "VIV"[9)] for simplicity in the present simulation. In this method, the particle phase is treated as a fluid whose density equals that of the solid, but an artificial body force $\bar{f}_p$ redistributes momentum within each particle at the end of a time step so as to recover rigid motion. Thus the particle-fluid system is treated as a variable-property fluid governed by the incompressible Navier-Stokes equations:

$$\frac{D(\rho\bar{u})}{Dt} = \nabla.(\bar{p} + \mu[\nabla\bar{u} + (\nabla\bar{u})^T]) + \rho\bar{g} + \bar{f}_p \quad (1)$$

$$\nabla \cdot \bar{u} = 0 \quad (2)$$

where ρ and μ are respectively density and viscosity, which are taken to vary between liquid and solid according to a somewhat smoothed distribution. In the VIV method, the artificial body force $\bar{f}_p$ is specified as:

$$\bar{f}_p(\bar{x}) = \alpha\rho\frac{(\bar{u}_p(\bar{x}) - \bar{u}(\bar{x}))}{\Delta t} \quad (3)$$

In this equation, α is the solid volume fraction and

$\bar{u}$ is the partial-step velocity in a grid cell where $\bar{u}_p = \bar{U}_p + \bar{\Omega}_p \times \bar{r}$ is the particle's target velocity at a grid point, $\bar{r}$ is the vector pointing from the particle center $\bar{X}_p$ to the cell center where $\bar{U}_p$ and $\bar{\Omega}_p$ are particle's translational and angular velocities.

(3) Particle- Particle interactions

To treat inter-particle contacts, and equivalently particle-wall contacts, we employed a DEM method[10] which is now briefly described. The normal and tangential components of contact force between particles *i* and *j* , denoted by the subscripts *n* and *t* respectively, are modeled as:

$$\bar{f}_{nij} = -\kappa_n \bar{\delta}_{nij} - (\eta_n \bar{v}_{rij} \cdot \bar{n}_{ij})\bar{n}_{ij} \qquad (4)$$

$$\bar{f}_{tij} = -(\kappa_t \bar{\delta}_{tij} + \eta_t \bar{v}_{sij}) \qquad (5)$$

where κ and η are stiffness and damping coefficients, $\bar{\delta}$ is the displacement vector, $\bar{v}_{rij}$ is the velocity of the particle *i* relative to particle *j*, $\bar{v}_{sij}$ is the slip velocity of the contact point and $\bar{n}_{ij}$ is the unit vector pointing from the center of particle *i* to that of particle *j*. When the tangential force $\bar{f}_{tij}$ satisfies $\left|\bar{f}_{tij}\right| > k\left|\bar{f}_{nij}\right|$, $\bar{f}_{tij}$ is replaced by:

$$\bar{f}_{tij} = -k\left|\bar{f}_{nij}\right| \bar{v}_{ij} / \left|\bar{v}_{ij}\right| \qquad (6)$$

where *k* is the coefficient of friction, taken to be 0.5 in the present simulations.

(4) Free surface modelling

The interface separated the liquid and air phases is also represented by a set of markers. Instead of satisfying boundary conditions at the free surface, we solve the fluid equations for the entire computational domain with variable density corresponded to the gas and liquid phases. Surface tension force evaluated at each interface element is added to the flow to maintain the shape of the interface. More details can be read in Tryggavson et. al paper[11].

(5) Numerical scheme

A finite-difference method based on a staggered grid and central differences in space is employed to solve the variable density Navier-Stokes equations[11]. Equation (1) is discretized from time level *n* to time level *n+1* by forward Euler method as:

$$\frac{\rho^{n+1}\bar{u}^{n+1} - \rho^n \bar{u}^n}{\Delta t} + \bar{A}^n = \bar{F}^n - \nabla \phi^{n+1} + \bar{f}^{n+1} \qquad (7)$$

where Δt is the time step, ϕ^{n+1} is the pseudo-pressure, $A^n = \nabla_h \cdot \rho^n \bar{u}^n \bar{u}^n$ is the momentum advection term and $\bar{F}^n = \nabla_h \cdot \mu^n (\nabla_h \bar{u}^n + \nabla_h{}^T \bar{u}^n) - \nabla_h p^n + \rho^n \bar{g}$ is the intensive fluid force.

Substeps for the fluid ("**F**") phase, particle ("**P**") phase, free surface ("**S**") and boundary ("**B**") are as follows:

P1) Update particle positions to t^{n+1} ,detect particle contacts and update particle velocity.

Because particles may contact at the time scale smaller than that of the fluid flow, we use shorter time interval for this step. Thus, to step a particle from time t^n to t^{n+1}, we need to perform *N* substeps which consist of the following tasks:

a)Advance particles from sub-step *k* to *k+1* as :

$$\bar{X}_p^{n+1,k+1} = \bar{X}_p^{n+1,k} + \Delta t \bar{U}_p^{n+1,k} \qquad (8)$$

b) Search for particle contacts, thereafter calculate the contact force $\bar{F}_c^{n+1,k+1}$ and torque $\bar{T}_c^{n+1,k+1}$. When the number of particles is large, this step is time consuming, therefore a suitable particle contact searching algorithm must be employed. In the present scheme, a cell linked list method[12] is used.

c)Calculate particle's translational and angular velocities at substep *k+1* as:

$$\bar{U}_p^{n+1,k+1} = \bar{U}_p^{n+1,k} + \frac{\Delta t}{N} \frac{\bar{F}_c^{n+1,k+1}}{M_p} \qquad (9)$$

$$\bar{\Omega}_p^{n+1,k+1} = \bar{\Omega}_p^{n+1,k} + \frac{\Delta t}{N} \frac{\bar{T}_c^{n+1,k+1}}{\bar{I}_p} \qquad (10)$$

P2)Based on the updated particle velocity, calculate the added force and update the fluid velocity field, and then calculate the new density and viscosity fields ρ^{n+1} and μ^{n+1}.

S1)Advect the free surface markers by local velocity interpolated at its location.

S2)Re-structure the connected markers by adding and/or deleting points and edge elements if necessary.

S3)Calculate the surface curvature and correspondingly, the force due to the surface tension

at the liquid-air interface; add to the momentum equation.

F1)Calculate the momentum advection term $\overline{A}^n$ and the intensive fluid force $\overline{F}^n$ in each momentum cell.

F2)Obtain the "fractional-step" momentum density $\rho^{n+1}\tilde{\overline{u}}$ by subtracting the momentum advection term $\overline{A}^n$:

$$\rho^{n+1}\tilde{\overline{u}} = \rho^n \overline{u}^n + \Delta t\left(\overline{F}^n - \overline{A}^n\right) \qquad (11)$$

and thence the fractional step velocity $\tilde{\overline{u}}$.

F3) Project $\tilde{\overline{u}}$ to obtain a solenoidal velocity field :

$$\tilde{\tilde{\overline{u}}} = \tilde{\overline{u}} - \frac{\Delta t}{\rho^{n+1}}\nabla\phi \qquad (12)$$

where ϕ satisfies the following elliptic equation :

$$\nabla_h \cdot \left(\frac{1}{\rho^{n+1}}\nabla_h \phi\right) = \frac{\nabla_h \cdot \tilde{\overline{u}}}{\Delta t} \qquad (13)$$

The pressure field is then updated by:

$$p^{n+1} = p^n + \phi^{n+1} \qquad (14)$$

P3)Within each particle, calculate the body force $\bar{f}_b$ by equation (3) and add to the fluid to yield a rigidified momentum density $\rho^{n+1}\overline{u}^{n+1}$

$$\rho^{n+1}\overline{u}^{n+1} = \rho^{n+1}\tilde{\tilde{\overline{u}}} + \Delta t\, \bar{f}_p^{n+1} \qquad (15)$$

B) Impose the target velocity at the drum boundary by calculating the body force $\bar{f}_b$ and adding it to the fluid as follows:

$$\bar{f}_b = \sum \delta(\overline{X}_m^b - \bar{x})\,\overline{F}_b(\overline{X}_m^b) \qquad (16)$$

The Lagrangian force at a marker is specified as:

$$\overline{F}_b(\overline{X}_m) = \rho_f h^3 \frac{(\overline{U}_b(\overline{X}_m^b) - \overline{U}(\overline{X}_m^b))}{\Delta t} \qquad (17)$$

where $\overline{U}(\overline{X}_m) = \sum \overline{u}\,\delta(\overline{X}_m - \bar{x})h^3$ is the fractional-step marker velocity which is interpolated from nearby grid cells by Peskin's[13] discretized Dirac delta function δ, h is the grid spacing; $\overline{U}_b(\overline{X}_m^b) = \overline{R}_m \times \overline{W}$; $\overline{R}_m = (X_m^b - X_G, Y_m^b - Y_G)$; $\overline{W} = (0,0,\Omega_b)$ and $\overline{X}_G = (X_l/2, Y_l/2)$ is the center and Ω_b is the angular velocity of the drum.

Table 1. Experimental conditions for two matched runs in the open drum, with up- and downstream boundary conditions changed somewhat as described in the text, and the resulting bed angle, clear-liquid flow depth h_t, and thickness t of the flowing grain layer. Values on the third line are results from 2D simulations.

Specific discharge q_f(cm^2/s)	Rotation rate Ω(rpm)	Bed angle θ (degree)	*h/d*	*t/d*
31.2	6.17	16.9	0.50	2.56
31.3	6.15	16.4	0.52	2.36
"	"	18.4	0.90	3.62

3. EXPERIMENT

(1) Apparatus

Figure 1 is a photograph of the rotating drum apparatus. The drum and flow tank sidewalls are made of acrylic plastic. The drum comprises two parallel circular plates, mounted on a steel axle with a separation between their inner surfaces of 2.2 cm, and which are sandwiched between the front and rear vertical sidewalls of the flow tank. A wire mesh forms a circumference, of inner diameter 19.32 cm, that joins the two plates near their edges; this mesh confines glass beads while allowing oil to flow in and out of the drum chamber. Oil is pumped from the tank at right to the upstream side, where an overflow weir is used to measure the flow rate with a beaker and stopwatch. Backflow under the tank is prevented by a plastic block whose upper surface is machined to a circular arc that fits the wire mesh, to a clearance of 0.05 cm, between an angles -55^O to the left, and + 35^O to the right, of vertical. The outer surfaces of the drum sidewalls are sealed with O-rings.

We report here on two runs; rotation rate and flow discharge are indicated in Tab 1. The main difference between the two runs was the boundary conditions in the upstream and downstream tank; the first run had a horizontal plate set at the height of the cusp of the sealing block, while the level in the downstream tank was much lower in the second run than the first. 450 beads of diameter 6.0 mm, and 200 of diameter 5.0 mm, were mixed to mitigate the formation of quasi-crystalline structure near the boundaries of the drum chamber. Temperature of the oil during experiments was 30.0 ±0.5 ^{0}C, for which density is 0.919 g/cm^3 and kinematic viscosity is 0.28 cm^2/s. Density of the beads is 2.440 g/cm^3.m^3.

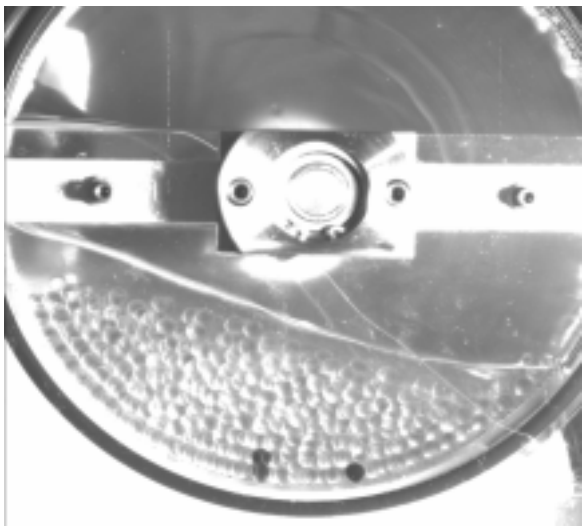

Fig. 3 Photograph of the experimental drum during the run on the second line of Table 1. Drum rotation is clockwise; oil flow is left to right. Three black tracer particles are visible.

A Kodak ES 1.0 camera, with 1008x956 pixel resolution, was used with stroboscopic illumination to image the whole drum at 30-frames/sec for runs of 702 images. Recording started after steady state was achieved.

(2) Image analysis

We focused on conditions in the "central section", defined as that where the normal ray to the bead bed passed through the central axis of the drum. The bead slope was determined visually at this section. Average bead velocity profiles where determined in the central section by visually tracking about ten black tracer particles (in the mixture of larger beads, only those of 6.0 mm diameter were marked). The region of interest was taken to be a narrow strip centered on the diameter perpendicular to the bead surface. The thickness t of the flowing layer was defined as the distance from the point of zero velocity (in the laboratory frame of reference) to the top of the flowing bead layer. The distance from the top of the bead layer to the free surface was called the flow depth, denoted h. The experimental values, as nondimensionalized by the bead diameter d, are reported in Tab. 1.

4. SIMULATION VS EXP. RESULTS

Photograph of the drum during the run on the second line of Tab.1 is shown in Fig. 3. Note first that the results for bed angle, flow depth, and thickness of the flowing bead layer were very close for the two experimental cases, which suggests that the detailed flow conditions up- and downstream barely affect results. Next, Fig. 4 shows an instance of fluid velocity field, bead distribution and the free surface from our 2D simulation of the case on the second line. Figure 5. shows the time evolution of the free surface. From the figures, the shape of the free surface (green curve) agrees well between simulation and experiment. The averaged velocity profiles for experiment and simulation determined visually and automatically, respectively, are over plotted in Fig. 6. The simulation's data is reported

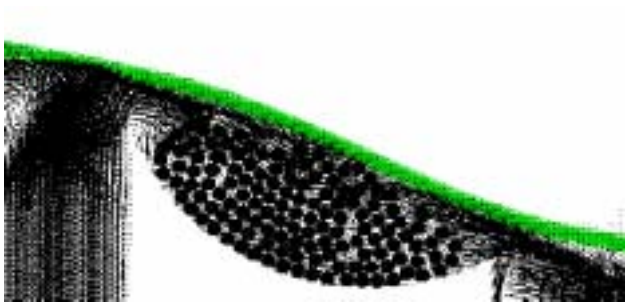

Fig. 4 Snapshot from 2D simulation corresponded to case 3) of the experiment., in conditions of third line of Tab. 1. Beads positions are shown as black disks, liquid velocity by arrows, free surface by the green curve.

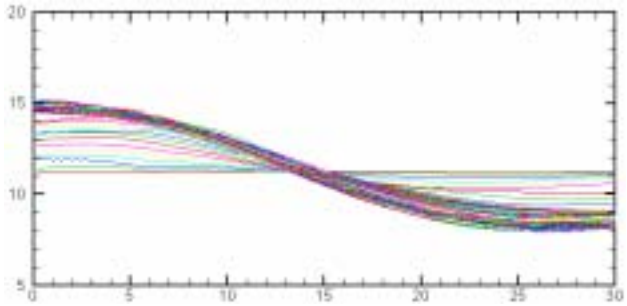

Fig. 5 Time evolution of the free surface from 2D simulation.

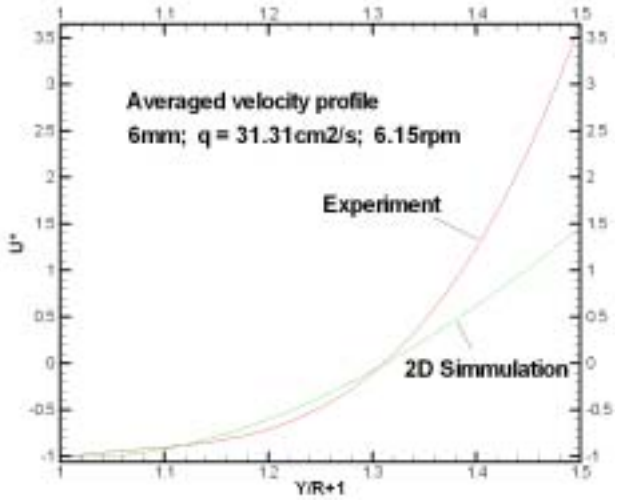

Fig. 6 Averaged bead velocity profiles determined from visually tracking tracer beads. Horizontal axis is height Y above drum circumference nondimensionalized by drum radius R.

on the third line in Tab. 1 Overall agreement is seen to be satisfactory for the bed slope, shape of the free surface, but there is a significant discrepancy in the thickness of the flowing grain layer, and furthermore a factor of about two between the maximum bead velocities (cf. Fig. 6). These differences may result from an "un-natural" resistance of simulated 2D granular assemblies to local deformation; shearing particles are forced to go over the tops of their neighbors, and the concomitant flow of liquid between pores is resisted by the narrow interparticle gaps.

5. CONCLUSIONS

We have designed and constructed a novel design of rotating tumbler that achieves a steady-state free-surface flow driving bedload transport within a limited space, thus providing a convenient benchmark for numerical simulations in nonequilibrium conditions. The present 2D simulation results agree well with corresponding experimental runs as concerns the form of the bead bed and free surface, and the thickness of the flowing bead layer, thus demonstrating the feasibility of our simulation method. However substantial differences were observed in peak bead velocity. These differences may result from an "un-natural" resistance of simulated 2D granular assemblies to local deformation; shearing particles are forced to go over the tops of their neighbors, and the concomitant flow of liquid between pores is resisted by the narrow interparticle gaps. These results allow us to hope that the fictitious-domain simulation method is indeed suitable for simulating dense-phase granular flow in a liquid. In the near future, we plan to perform corresponding 3D simulations, like those already performed - though with no free surface - in reference (5).

ACKNOWLEDGMENTS: We thank Prof. S. Egashira and Prof. T. Itoh for helpful discussions. Graduate student Thien Duy NGUYEN assisted with experiments.

REFERENCES

1) Werner, B.T., Haff, P.K., The impact process in aeolian saltation: Two-dimensional simulations, *Sedimentology*, 35, 189-196, 1988.

2) Schmeeckle, M. W., The Mechanics of Bedload Sediment Transport: Ph.D. dissertation, Univ. of Colorado, 158 p, 1998.

3) Gotoh, H., Harada, E., Sakai, T.: Movable bed simulator for fractional transport of graded sediment,*水工学論文集*, Vol. 44, 665-670,2000

4) Drake, T.G., Calantoni J. : Discrete particle model for sheet flow P.K.on the near shore, *Journal of Geophysical Research - Oceans*, 106-C9, 19859-19868,2001.

5) Truong, H, Wells, J., Nguyen, Anh An experimental check on particle dynamics simulations of erodible particle beds; the rotating tumbler,*水工学論文集*, Vol. 50,2006

6) Kajishima, T., Takiguchi, S. : Interaction between particle clusters and particle-induced turbulence, *Int.J. Heat Fluid Flow* 23, 639-646, 2002

7) Uhlmann, M.: An immersed boundary method with direct forcing for the simulation of particulate flows, *J. Comput. Phys.* , 209,448-476, 2005.

8) Truong, H.V., Wells, J.C. , Tryggvason, G. : Explicit vs. implicit particle-liquid coupling in fixed-grid computations at moderate particle Reynolds number, FEDSM2005-77206, *ASME FED Summer Meeting*, June 19-23,2005, USA

9) Truong, H.V., Wells, J.C. , Tryggvason, G. : Implicitly - coupled finite diference schemes for fictitious domain simulation of solid-liquid flow; marker, volumetric, and hybrid forcing, *ERCOFTAC workshop*, DLES6 Sept.,2005, France.

10) Tsuji, Y., Tanaka, T., Ishida, T. Lagrangian numerical simulation of plug flow of cohesionless particles in horizontal pipe, *Powder technology* 71, pp 239-250, 1992.

11) Tryggvason, G., Brunner, B., Esmaeeli, A., Juric, D., Alrawashi, N., Tauber, W., Han, J., Nas, S., Jan, Y.J. : A front tracking method for the computations of multiphase flow, *J. Comput. Phys.*, 169, 708-759, 2001.

12) Allen, M.P., Tildesley, D. : Computer simulation of liquids, Clarendon Press, Oxford 1987.

13) Peskin, C.S., The immersed boundary method, *Acta numerica*, 11, 479-517, 2002.

(Received September 30, 2006)